Ultrasensitive, Biocompatible, Quantum-Dot-Embedded Silica Nanoparticles for Bioimaging

Bong-Hyun Jun, Do Won Hwang, Heung Su Jung, Jaeho Jang, Hyunsoo Kim, Homan Kang, Taegyu Kang, San Kyeong, Hyeokjae Lee, Dae Hong Jeong, Keon Wook Kang, Hyewon Youn, Dong Soo Lee, and Yoon-Sik Lee**

The successful development of highly sensitive, water-compatible, nontoxic nanoprobes has allowed nanomaterials to be widely employed in various applications. The applicability of highly bright quantum dot (QD)-based probes consisting of QDs on 120 nm silica nanoparticles (NPs) with silica shells is investigated. Their substantial merits, such as their brightness and biocompatibility, for effective bioimaging are demonstrated. Silica-coated, QD-embedded silica NPs (Si@QDs@Si NPs) containing QDs composed of CdSe@ZnS (core-shell) are prepared to compare their structure-based advantages over single QDs that have a similar quantum yield (QY). These Si@QDs@Si NPs exhibit approximately 200-times stronger photoluminescence (PL) than single QDs. Cytotoxicity studies reveal that the Si@QDs@Si NPs are less toxic than equivalent numbers of silica-free single quantum dots. The excellence of the Si@QDs@Si NPs with regard to in vivo applications is illustrated by significantly enhanced fluorescence signals from Si@QDs@Si-NP-tagged cells implanted in mice. Notably, a more advanced version of QD-based silica NPs (Si@mQDs@Si NPs), containing multishell quantum dots (mQDs) composed of CdSe@CdS@ZnS, are prepared without significant loss of QY during surface modification. In addition, the Si@mQDs@Si NPs display a fivefold higher fluorescence activity than the Si@QDs@Si NPs. As few as 400 units of Si@mQDs@Si-NP-internalized cells can be detected in the cell-implanted mouse model.

1. Introduction

Semiconductor nanoparticles (quantum dots (QDs)) have great potential in both fundamental research and applied fields due to their specific optical and electronic properties based on quantum confinement effects.[1,2] The fluorescence and emission properties of QDs can be varied over a broad range of the electromagnetic spectrum by a simple adjustment of the particle size. The high fluorescence quantum yield (QY) and high optical stability of QDs in comparison with their counterparts, such as organic fluorescent molecules and phosphor dyes, make them potentially promising nanomaterials for photovoltaic cells,[3,4] biosensors[5] and light-emitting diodes.[6] Especially, with respect to bioapplications, they provide unrivalled cellular imaging and therapeutic detection capabilities. However, the practical application of QDs to biofields is hampered by some key limitations relating to surface modification and safety issues.[7,8] A useful method for overcoming these problems

Dr. B.-H. Jun,[+] T. Kang, S. Kyeong, Prof. Y.-S. Lee
School of Chemical and Biological Engineering
Seoul National University
Seoul, 151-747, Korea
E-mail: yslee@snu.ac.kr
Dr. D. W. Hwang, Prof. K. W. Kang, Prof. H. Youn, Prof. D. S. Lee
Department of Nuclear Medicine
Seoul National University College of Medicine
Seoul, 110-744, Korea
E-mail: dsl@snu.ac.kr
Dr. D. W. Hwang
Institute of Radiation Medicine
Medical Research Center
Seoul, 110-744, Korea
Dr. H. S. Jung, H. Kim, H. Lee
Nanosquare Inc. ENG BLD39-122
Seoul National University
Seoul, 151-747, Korea

DOI: 10.1002/adfm.201102930

J. Jang, Prof. D. S. Lee
WCU Department of Molecular Medicine and Biopharmaceutical Sciences, Graduate School of Convergence Science and Technology
Seoul National University, Seoul, 151-747, Korea
H. Kang, Prof. D. H. Jeong, Prof. Y.-S. Lee
Nano Systems Institute and Interdisciplinary Program in Nano-Science and Technology
Seoul National University
Seoul, 151-747, Korea
Prof. D. H. Jeong
Department of Chemistry Education
Seoul National University, Seoul, 151-747, Korea
Prof. H. Youn
Cancer Imaging Center
Seoul National University Cancer Hospital
Cancer Research Institute
Seoul National University College of Medicine
Seoul, 110-799, Korea
[+] Present address: Department of Bioengineering
University of California Berkeley, Berkeley, CA 94720, USA

is silica encapsulation, which confers many advantages, such as water compatibility, facile chemical modification, low cytotoxicity and excellent chemical stability. Thus far, many studies for the development of silica-encapsulated QDs have been published.[9–12] They employ single QDs for encapsulation with the goal of obtaining a high QY for brighter and more sensitive detection.

Nanoprobes containing multiple QDs have also been developed for better optical characteristics and good biocompatibility.[13–16] When silica NPs are used as a template for embedding QDs, they can provide additional advantages, such as easier control of size and multifunctional properties. Multiple-QD-containing units can be brighter than single QDs due to their greater number. However, the QY of QDs becomes relatively lower when multiple QDs are introduced on silica NPs. Thus, the development of QD nanomaterials possessing high QY and excellent biocompatibility is required for highly sensitive in vivo applications.

Nanoprobes containing multiple QDs carrying multiple components, such as targeting ligands or antibodies, have been intensively studied for in vivo diagnosis or therapy; however, methods for enhancing the QY through nanostructural aspects need to be systemically studied.[17,18]

Herein, we report highly bright QD-embedded silica NPs (Si@QDs@Si NPs) for bioimaging. We have developed a method for embedding QDs onto a carrier template so that a large number of hydrophobic QDs can be attached to hydrophilic silica NPs. We have also demonstrated the key advantages of Si@QDs@Si NPs, compared with single QDs, in terms of brightness and toxicity. Multishell QD (CdSe@CdS@ZnS) (mQD)-embedded NPs (Si@mQDs@Si NPs) have also been prepared to compare with the Si@QDs@Si NPs in terms of QY. They have better optical characteristics than the Si@QDs@Si NPs for sensitive in vivo cell tracking.

2. Results and Discussion

2.1. Design of QD- and mQD-Embedded Silica NPs

The fabrication flow of the proposed, highly bright, silica-coated quantum-dot-embedded silica NPs (Si@(QDs or mQDs)@Si NPs) is illustrated in **Scheme 1**. The diameter of the silica-core NPs was approximately 120 nm. QDs were embedded on the surface of silica NPs, a carrier template, for easy handling and size control, and reproducible preparation of nanomaterials. Then, they were encapsulated by a silica shell to provide biocompatibility and easy functionalization. Here, two types of QD were used to yield different types of nanoprobe: core-shell CdSe@ZnS QDs (QDs) and core-multishell CdSe@CdS@ZnS QDs (mQDs).

Monodisperse QDs (CdSe@CdS) that had a narrow photoluminescence (PL) emission (full-width at half maximum (FWHM) = 37.8 ± 1.0 nm wavelength) and a high PL efficiency were prepared by a one-pot process.[19–21] The photoluminescence maxima of the QDs varied from 450 to 650 nm depending on the precursor ratio (Figure S1a,b, Supporting Information). They exhibited high fluorescence quantum yields reaching up to 80%. They displayed monodisperse sizes of approximately 6 nm

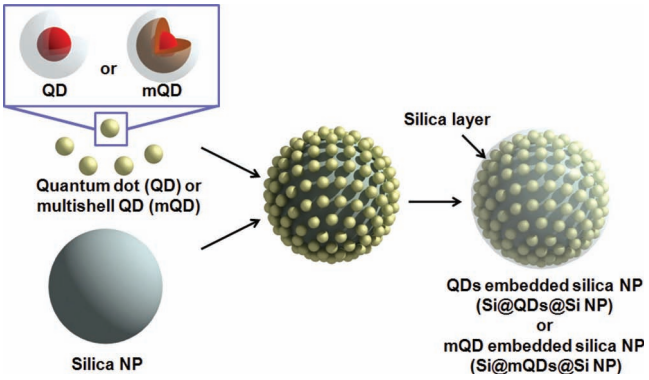

Scheme 1. Illustration of synthesis of silica-coated (QD or mQD)-embedded silica NPs. Core-shell CdSe@ZnS QDs (QDs) and core-multishell CdSe@CdS@ZnS QDs (mQDs) are immobilized to thiol-modified silica NPs; then, Si@QDs@Si NPs and Si@mQDs@Si NPs are prepared by silica-shell encapsulation.

diameter by controlling the shell thickness in a sub-kilogram scale synthesis (Figure S1c–d, Supporting Information). However, the quantum yields of the red-PL QDs were reduced from 64% to 18% after surface ligand exchange with 3-mercaptopropionic acid (MPA), which was necessary for the QDs to become water compatible so that they could be compared with the silica-coated QD–embedded silica NPs (Si@QDs@Si NPs).

Core-multishell QDs composed of CdS@CdS@ZnS (mQDs) were also prepared to protect the QD surface during surface ligand exchange. Detail synthesis methods are described in the supporting information. The synthesized quantum dots exhibited tunable photoluminescence maxima when the precursor amounts were controlled. The diameters of the mQDs were approximately 9 nm (Figure S2a, Supporting Information) and the mQDs possessed a similar QY to the core-shell QDs. However, the prepared mQDs sustained their QY from 85% to more than 95% after MPA ligand exchange. The ligand-exchanged mQDs are shown in Figure S2b,c, Supporting Information. Colloidal solutions of the mQDs remained clear with no signs of precipitation, even after standing at room temperature for 6 months. The photostability was tested by exposing the two types of QD in toluene to different UV doses (1000, 2000, and 3000 mJ cm^{-2}), which did not hamper their stability, and their fluorescence intensities remained practically unchanged (Figure S2d, Supporting Information).

To prepare the Si@QDs@Si NPs, 120 nm silica NPs were prepared by the Stöber method and used as a carrier template for the QDs (Figure S3, Supporting Information). The embedding of a large number of hydrophobic QDs to cover the entire surface of the hydrophilic silica backbone was challenging. The silica NPs were functionalized with a thiol group using mercaptopropyl trimethoxysilane (MPTS) as an organosilane coupling agent, because they have a high affinity to QDs. The thiol-functionalized silica NPs, however, exhibited hydrophilic properties, whereas the QDs, which had a trioctylphosphine (TOP) layer, possessed hydrophobic properties. To embed the hydrophobic QDs onto the hydrophilic thiol-modified silica NPs, we controlled the amounts of each solvent for the silica NPs and QDs in order to achieve efficient mixing, instead of using an

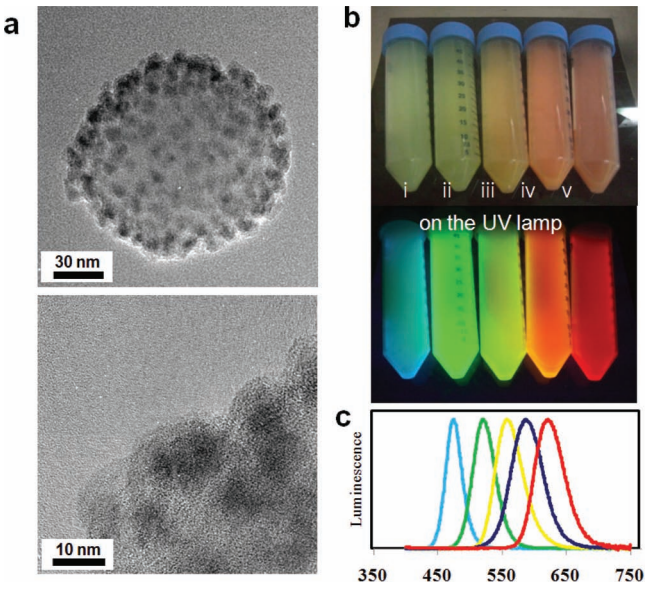

Figure 1. Characterization of Si@QDs@Si NPs. a) TEM images of Si@QDs@Si NPs – multi units of QDs (500 QDs) were embedded on a silica NP and a thin silica layer was formed around the QD-embedded silica NP. b) Photographs of various Si@QDs@Si NPs from QDs with emission maxima at 470, 520, 550, 580 and 615 nm under daylight and UV light. c) The PL emission of the corresponding Si@QDs@Si NPs.

amphiphilic polymer,[22] which can reduce the QY upon further silica-shell coating. The QD-embedded silica NPs were collected for analysis by centrifugation. High-resolution transmission electron microscopy (HR-TEM) analysis revealed that the QD-embedded silica NPs had rough surfaces, most likely due to the embedding of QDs on the surface of the silica core (Figure S4a, Supporting Information). The lattice structure of the QDs could be observed on the surface of the silica NPs (Figure S4b, Supporting Information). The number of QDs on the silica core was estimated to be ≈200–300 per single 120 nm silica NP.

The PL signal of one unit of a QD-embedded silica NP could be amplified by increasing the number of embedded QDs. Therefore, when MPTS, which can be self-assembled onto QDs and acts as a silica-shell precursor, was further added to the QDs and the QD-embedded silica-NP mixture, most of the free QDs were further embedded on the silica NPs. The MPTS-treated QD-embedded silica NPs were dispersed in ethanol (EtOH). They were then encapsulated by a silica shell with tetraethyl orthosilicate (TEOS). As shown in **Figure 1**a, approximately 500 QDs were embedded on each silica NP, and a thin silica layer was formed around the QD-embedded silica NPs. The Si@QDs@Si NPs did not coagulate during the silica-coating step, and were well dispersed in water, possessing characteristic PL properties (Figure 1b,c, **Table 1** and Figure S5, Supporting Information). Energy-dispersive X-ray (EDX) and inductively coupled plasma (ICP) analyses confirmed the presence of elements such as Cd (data not shown).

2.2. Assessment of QY in Various Types of Si@QDs@Si NP

Various QDs with similar diameters of approximately 6 nm were embedded on 120 nm silica NPs (Figure 1). The resulting

Table 1. Wavelength, band width and QY of various QDs.

	Wavelength [nm]		FWHM [nm]		QY [%]		
	QDs	Si@QDs@Si NPs	QDs	Si@QDs@Si NPs	QDs	Si@QDs@Si NPs	Nomalized QY
1	471	475	29	29	52	18	35
2	517	521	38	41	62	32	52
3	556	558	40	49	62	31	50
4	574	587	47	57	60	33	55
5	612	622	43	53	63	13	21

Si@QDs@Si NPs exhibited slight spectral changes (red shift) and an increased bandwidth as compared with bare QDs, as can be inferred from Table 1. The remaining QYs (normalized QY from bare QDs) of the Si@QDs@Si NPs were comparable with those of the QDs, with emission maxima at 471, 517, 556, 574 and 612 nm, and were estimated to be 35, 52, 50, 55 and 21%, respectively.

Here, a notable decrease in the QY of the red Si@QDs@Si NPs was observed, most likely due to the thinner shells in the red QDs (emitting at approximately 600 nm) than in the green QDs. We prepared different types of red Si@QDs@Si NP to obtain higher QYs. QDs with a thicker ZnS shell were stable after surface ligand exchange and surface tuning, and had a higher QY. When the molar ratio of the ZnS shell (Cd:Zn) was changed from 1:4.4 to 1:5.8, the QY of the QDs increased from 21% to 38%. However, the preparation of CdSe@ZnS QDs with a thicker ZnS shell was problematic with respect to fabrication, and less loading on the silica NPs was achieved. Although the Si@QDs@Si NPs gave a reasonable QY for bioapplications, the red Si@QDs@Si NPs exhibited a relatively low QY during QD embedding.

We also prepared core-multishell-type red QDs (mQDs) that had a QY of 64%. Thus, the Si@mQDs@Si NPs, which had mQDs instead of QDs, were prepared by a similar immobilization method. We found that the prepared Si@mQDs@Si NPs maintained the initial QY of the mQDs almost quantitatively. Moreover, the resulting Si@mQDs@Si NPs possessed approximately 500 mQDs and had a high QY of 64%. Their photoluminescence activity was intact over 2 months.

2.3. Highly Sensitive Quantum-Dot-Embedded Silica Nanoparticles (Si@QDs@Si NPs) for in vivo Cell Tracking

To compare the fluorescence intensity of one Si@QDs@Si NP, which had approximately 500 units of single QDs, with that of a single QD (sQD),[23] luminescence signals from the Si@QDs@Si NPs and an equivalent number of sQDs were examined in an Eppendorf tube. Luminescence images of the tubes revealed significantly amplified luminescence activity of the Si@QDs@Si NPs compared with the sQDs (**Figure 2**a). Quantitative fluorescence analysis using a fluorometer showed a fluorescence intensity from the Si@QDs@Si NP samples approximately 200-times higher than that from the sQD samples (Figure 2b). In order to verify the efficiency of the Si@QDs@Si NPs during

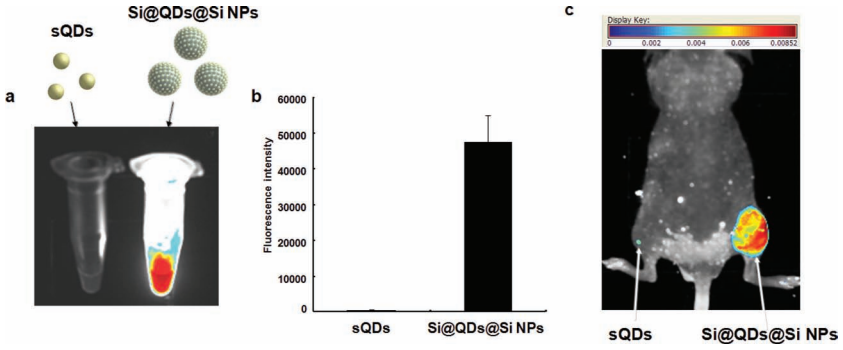

Figure 2. Comparison of fluorescence intensities of sQDs and Si@QDs@Si NPs. a) Fluorescence images of tubes containing sQDs (left) and Si@QDs@Si NPs (right). b) Quantitative analysis of the sQDs (left) and Si@QDs@Si NPs (right). c) Fluorescence image of a BALB/c nude mouse where sQDs (left) or Si@QDs@Si NPs (right) (2 pmol) were injected.

in vivo experiments, Si@QDs@Si NPs and sQDs resuspended in 150 μL of phosphate buffered saline (PBS) were subcutaneously administered respectively into the thighs of a mouse. Much brighter in vivo fluorescence was observed in the right thigh of the mouse that was injected with the Si@QDs@Si NPs compared with the left thigh, which was injected with the sQDs (Figure 2c). Subsequently, the Si@QDs@Si NPs were applied to a cellular system to verify their usefulness for in vivo cell tracking.

To confirm whether the natural uptake of Si@QDs@Si NPs occurred in cells, comparable amounts of both the Si@QDs@Si NPs and the sQDs were incubated in Henrietta Lacks (HeLa) cells for 24 h, as illustrated in **Figure 3**a. Confocal microscopy images confirmed that most of the Si@QDs@Si NPs were distributed in the cytoplasmic area of cells (Figure 3b). The transfection efficiency of the Si@QDs@Si NPs in cells was analyzed 24 h after transfection. The fluorescence signals in the supernatant and in the trypsinized-cell pellets were measured using a fluoremeter. We found that the transfection efficiency in the Si@QDs@Si-NP-transfected cell pellets was 88%. Nanomaterials of appropriate size are known to be allowed for intracellular uptake by natural endocytosis. We confirmed that the 120 nm-sized Si@QDs@Si NPs could accumulate easily inside the cells without cell-penetrating peptides such as trans-activator of transcription (TAT).[24] Indeed, we found that endocytic uptake of the Si@QDs@Si NPs into the HeLa cells occurred in 3 h after treatment, based on the fluorescence signal, by confocal microscopy, in the cytoplasmic area (data not shown).

To prove the biological usefulness of Si@QDs@Si NPs for in vivo cell tracking, the same number of sQDs and Si@QDs@Si NPs were mixed with preseeded HeLa cells in a 10 cm flask dish. After incubation of the cells with sQDs and Si@QDs@Si NPs for 24 h, the collected HeLa cells were subcutaneously implanted into the left thigh (sQDs containing HeLa cells) and the right thigh (Si@QDs@Si NPs containing HeLa cells) of a nude (nu/nu) mouse. Intense fluorescence activity was observed from Si@QDs@Si-NP-labeled cells as soon as they were injected, whereas the sQD-treated cells, which were injected in the left thigh of the mouse, did not exhibit any in vivo fluorescence (Figure 3c). The intensity of the fluorescence signal from the Si@QDs@Si-NP-labeled cell-implantation site gradually decreased with time because the Si@QDs@Si NPs in the cells were diluted in the process of cell proliferation.

Numerous imaging approaches for reporter-based or NP-based cell tracking have been implemented to understand the migration characteristics of therapeutically implanted cells.[25–26] Reporter-based strategies for cell tracking, however, may induce potential side effects such as insertional mutagenesis. Furthermore, the NP-based cell-tracking method affords only limited long-term cell tracking due to the gradual dilution of the nanomaterials in cells. Thus, nanomaterials can be used as cell trackers for in vivo studies taking less than 10 d. Cell tracking using nanomaterials has

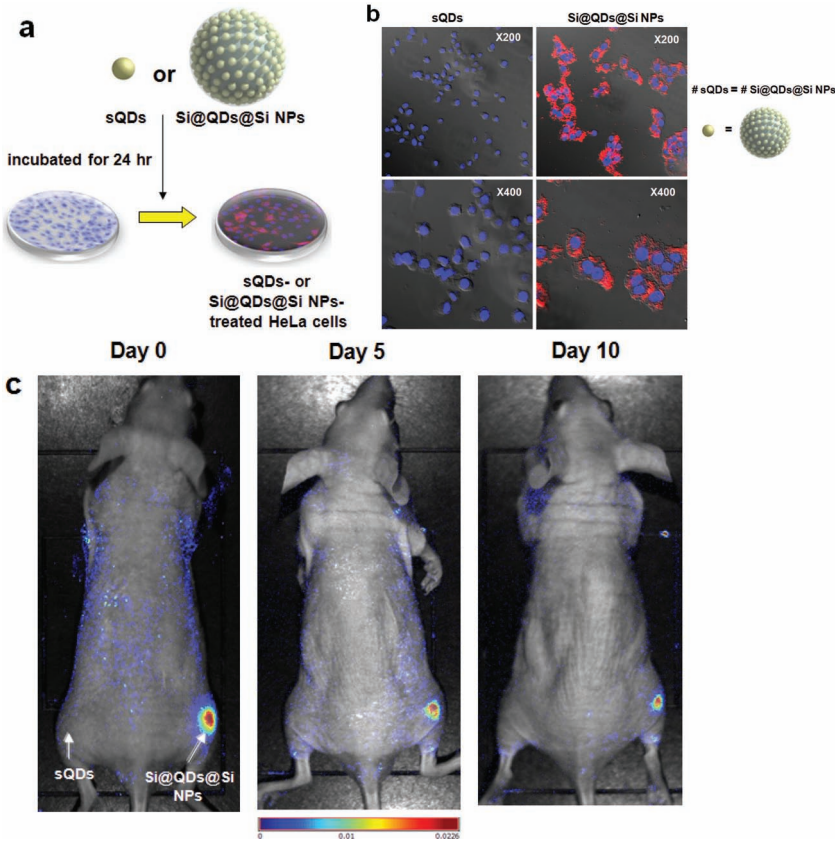

Figure 3. Cellular uptake in vivo test of sQDs and Si@QDs@Si NPs. a) Illustration of sQD or Si@QDs@Si-NP labeling to HeLa cells. b) Fluorescence images of sQD- and Si@QDs@Si-NP-uptaken cells (Red color: QD, blue color: DAPI). c) Maestro in vivo fluorescence image of sQD-labeled (left leg) and Si@QDs@Si-NP-labeled (right leg) cell-transplanted mouse.

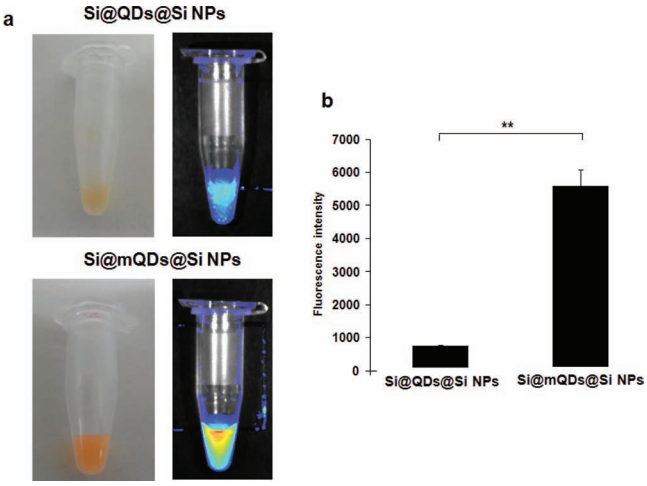

Figure 4. Comparison of the Si@mQDs@Si NPs with the Si@QDs@Si NPs. a) Fluorescence images of the Si@mQDs@Si NPs and the Si@QDs@Si NPs. b) Quantitative measurements of the fluorescence signals of the Si@mQDs@Si NPs and Si@QDs@Si NPs.

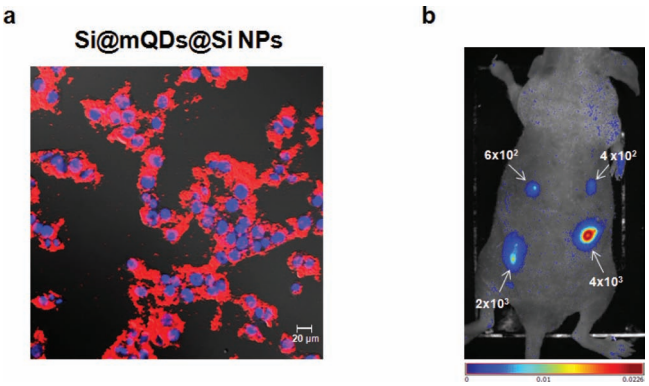

Figure 5. Visualization of highly bright Si@mQDs@Si NPs. a) Fluorescence image of Si@mQDs@Si-NP-uptaken HeLa cells (0.5 mg in 1 × 10^6 cells). b) Fluorescence image of different numbers of cells injected into a mouse.

recently drawn much attention in terms of its safety.[27,28] Therefore, nontoxic and highly bright Si@QDs@Si NPs are suitable candidates for cell tracking.

2.4. In Vivo Fluorescence-Detection Range of Si@mQDs@Si NPs in a Cancer-Cell-Implanted Mouse Model

We also investigated the biological usefulness of our newly developed Si@mQDs@Si NPs, which have a similar structure but exhibited a better QY than the Si@QDs@Si NPs. In PBS solvent, the Si@mQDs@Si NPs showed a clearer orange color when compared with the Si@QDs@Si NPs (**Figure 4**a). When the fluorescence images were compared using the same amounts of Si@mQDs@Si NPs and Si@QDs@Si NPs (0.1 mg), the Si@mQDs@Si NPs showed a brighter fluorescence activity (Figure 4a). Being consistent with the fluorescence images, quantitative analysis using a fluorometer showed that the Si@mQDs@Si NPs samples had an approximately 5-fold higher fluorescence activity than an identical amount of Si@QDs@Si NPs (Figure 4b). To verify whether the Si@mQDs@Si NPs were also internalized into the intracellular area, Si@mQDs@Si NPs (0.5 mg) resuspended in PBS buffer were treated in HeLa cells for 24 h.

As shown in **Figure 5**a, confocal microscopy revealed that internalization of the Si@mQDs@Si NPs occurred in the HeLa cells, showing significantly bright fluorescence signals in the cytoplasmic area. We verified that approximately 120 nm-sized Si@mQDs@Si NPs were also internalized into the cells through general endocytosis. Once the presence of Si@mQDs@Si NP-tagged cells was confirmed, we then investigated the minimum number of Si@mQDs@Si NP-tagged cells that could be detected in vivo. Si@mQDs@Si-NP-tagged HeLa cells were prepared after incubation with Si@mQDs@Si NPs (5 mg) in a 10 cm dish for 24 h. The harvested cells were injected subcutaneously into four areas of the skin in a cell-number-dependent manner. From in vivo fluorescence imaging, we could detect up to 1000 cells in the Si@mQDs@Si-NP-injected mouse group (Figure 5b), demonstrating that visualization of as few as 400 units of Si@mQDs@Si-NP-labeled cells was possible for tracking a variety of cell migration patterns in the subcutaneous region of the mouse.

The Si@mQDs@Si NPs have substantial merits. They are monodisperse, nontoxic due to the silica coating, highly sensitive with a bright fluorescence intensity (high QY), and they are easily taken up into cells. Even a small number of cells implanted into mice could be detected with Si@(QDs or mQDs)@Si NPs. They can be further utilized in a variety of biological systems such as for stem cell research or in vivo immune cell tracking.

A cancer-targeted imaging approach using sQDs was reported recently.[29,30] Nevertheless, the fluorescence-based detection method still has a tissue penetration problem, which may hamper accurate cancer diagnosis. Although newly developed 600 nm-emitting Si@mQDs@Si NPs are highly bright, fluorescence attenuation in deep tissue remains a challenge. To overcome this, we are currently developing near-IR-emitting Si@mQDs@Si NPs. Further refinement of our system will enable us to develop efficient in vivo cancer-targeting nanomaterials.

3. Conclusions

We have developed a synthetic method to prepare highly luminescent (high PL efficiency) and monodisperse (narrow PL emission) semiconductor QDs, as well as QDs with a thicker ZnS layer, which protects the QD surface during surface ligand exchange and surface tuning. We have also synthesized highly bright QD-embedded nanoprobes (Si@QDs@Si NPs and Si@mQDs@Si NPs) by embedding a large number of hydrophobic QDs onto the surface of hydrophilic silica NPs. Using this technique, a gram-scale quantity of water-compatible Si@QDs@Si NPs was successfully prepared, and the material exhibited a low toxicity and 200-fold stronger PL emission than single QDs. We also confirmed the suitability of Si@QDs@Si NPs for in vivo use by monitoring the highly amplified fluorescence signals from Si@QDs@Si-NP-tagged cells for 10 d. By applying multishell

QDs, highly bright Si@mQDs@Si NPs containing approximately 500 mQDs were prepared without loss of QY (QY 64%). The structural changes in the Si@mQDs@Si NPs, which contained multilayered QDs (CdSe@CdS@ZnS), resulted in an enhanced fluorescence activity with a high QY, allowing the detection of as few as 400 Si@mQDs@Si-NP-labeled cells in mouse skin. Thus, Si@mQDs@Si NPs are proven to be useful in biomedical fields, particularly for the bioimaging of in vivo cell tracking, which requires a high sensitivity.

4. Experimental Section

Preparation of CdSe@ZnS QDs: Cadmium oxide (CdO) (99.99%), selenium (99.9%, powder), zinc dimethyldithiocarbamate ($Zn(DMSC)_2$) (97%, powder), trioctylphosphine (TOP) (90%), oleic acid (OA) (90%) and 1-octadecene (ODE) (90%) were purchased from Sigma–Aldrich and used as received. CdO (1×10^{-3} M, 0.1284 g) and $Zn(DMSC)_2$ (5×10^{-3} M, 1.520 g) were dissolved in OA (1.695 g) and ODE (20 mL), treated with N_2 gas, and heated to 100 °C under vacuum for 1 h. The solution was further heated to 320 °C to form a transparent solution and injected into a precursor solution, which was prepared by dissolving Se (1×10^{-3} M, 0.078 g) in TOP (1 mL). The growth temperature was set to 300 °C for 5 min and then the solution was cooled to room temperature.

The QDs exhibited superior, stable optical properties, without any observed decrease after being exposed to UV radiation for 3000 h. Moreover, sub-kilogram scale quantities of CdSe@ZnS nanocrystals could be obtained using a larger reactor volume and increased amounts of precursors and solvents (Figure S1d, Supporting Information).

Preparation of Multishell QDs (mQDs): The metal precursor solution was prepared by dissolving CdO (0.205 g) in OA (10 mL) and ODE (60 mL), treating with N_2 gas and heating at 200 °C under vacuum for 1 h. The solution was further heated to 320 °C to form a transparent solution and injected into a precursor solution of Se (0.025 g) dissolved in TOP (1.6 mL). After 100 s, octanethiol (0.32 mmol) was added to the reaction mixture dropwise at a rate of 1 mL min^{-1}. After 30 min, a Zn precursor solution, prepared by dissolving zinc acetate (0.587 g) and OA (5 mL) in ODE (10 mL) at 300 °C under an N_2 atmosphere, was injected into the reaction mixture. Sulfur (0.103 g) dissolved in 2 mL of TOP was injected rapidly into the mixture. The final solution was heated at 320 °C for 5 min and cooled to room temperature, affording the mQDs.

Preparation of Water-Soluble Single QDs: Purified QDs or mQDs were dispersed in $CHCl_3$ to obtain a 0.1×10^{-6} M QD solution. Tetramethylammonium hydroxide (TMAH) (100 mg) was mixed well with 3-mercaptopropionic acid (MPA) in 1 mL of $CHCl_3$. The amount of MPA was varied between 5 and 100 µL to determine its effect on the ligand-exchange reaction. After 15 min, a clear, colorless, aqueous layer (about 10% of total volume) formed above the $CHCl_3$ layer. The biphasic solution was mixed by vigorous shaking and was allowed to stand for 1 h in order to equilibrate. The lower organic phase, which contained deprotonated MPA, was transferred into a vial for the ligand-exchange reaction with the QDs or mQDs. 100 µL of TOP-capped QDs (0.1 µM in $CHCl_3$) were added to the MPA-$CHCl_3$ solution and mixed well. The solution was allowed to stand at room temperature for 1–5 h. After the reaction, the MPA-capped QDs that had separated from the $CHCl_3$ solutions were collected, washed with $CHCl_3$ (three times), and dispersed in 1.0 mL of water.[22]

Preparation of QD-Immobilized Thiol-Modified Silica NPs: Silica NPs were prepared by the well-known Stöber method. A 3 mL portion of ammonium hydroxide (27%) was added to 40 mL of EtOH, which contained 1.6 mL of tetraethylorthosilicate (TEOS), accompanied by vigorous magnetic stirring for 20 h at 25 °C. The silica NPs were centrifuged and washed several times with EtOH. These silica NPs were then thiol functionalized with 3-mercaptopropyltrimethoxysilane (MPTS). The silica NPs (300 mg) were dispersed in 6 mL of EtOH containing 60 µL of MPTS and 150 µL of ammonium hydroxide. The mixture was stirred for 12 h at 25 °C. The resulting MPTS-treated silica NPs were centrifuged and washed with EtOH several times.

The QDs (3 mL, 30 mg mL^{-1} in $CHCl_3$) were transferred to a vial, and most of the hydrophobic solvent ($CHCl_3$) was evaporated under vacuum. Silica NPs (2 mL, 50 mg mL^{-1} in EtOH) were then added to the concentrated QD suspension. Because the QDs were hydrophobic, they were precipitated in the hydrophilic EtOH. The fluidic silica NPs came into contact with the QDs upon shaking of the mixture for a few seconds, and the resulting QD-embedded silica NPs were precipitated in the EtOH, owing to the hydrophobic nature of the QD-embedded silica NPs. $CHCl_3$ (20 mL) was subsequently added to the suspension, which was shaken to reinforce the immobilization of the QDs onto the silica NPs. After shaking for 5 min, 20 mL of $CHCl_3$, 1 mL of MPTS and 1 mL of NH_4OH were added to the mixture. After shaking for 1 h, the resulting mixtures were centrifuged and washed with EtOH several times, after which the collected mixture was well dispersed in 40 mL of EtOH, 1 mL of TEOS and 1 mL of NH_4OH. After shaking for 12 h, the resulting mixtures were centrifuged and washed with EtOH several times.

In Vitro Luminescence Signal Acquisition: Si@QDs@Si NPs (1.1×10^{12} per mL; stock concentration = 5 mg mL^{-1}) suspended in absolute EtOH were centrifuged at 6500 rpm for 1 min to exchange the EtOH solvent for PBS solution. Si@QDs@Si NPs or sQDs (100 µg per 20 µL) in PBS solution were added to a dark 96-well microplate, and the fluorescence signal was detected using an Infinite M200 Fluorometer (Tecan, GmbH, SZ, Austria) at optimized excitation/emission wavelengths of 400/610 nm. The fluorescence signal intensities of each sQD- or Si@QDs@Si-NP-containing well plate were normalized to those of a PBS-containing well plate.

Cytotoxicity Studies: HeLa cells, human cervical carcinoma, which were maintained in Dulbecco's modified Eagle medium (DMEM) (Gibco, Grand Island, NY) containing fetal bovine serum (FBS) (Invitrogen, Grand Island, NY), 10 U mL^{-1} penicillin (Invitrogen, Grand Island, NY) and 10 µg mL^{-1} streptomycin, were inoculated in a 96-well microplate, and sQDs or Si@QDs@Si NPs of increasing concentration, ranging from 10 to 40 µg, were transferred to the seeded HeLa cells. After incubation for 24 h at 37 °C, the cellular toxicity was examined using a simple cellular toxicity kit, cell counting kit-8 (CCK-8) (Dojindo Molecular Tech, Inc, Rockville). The incubated cell medium was clearly removed via a PBS washing step, and 10 µL of the CCK-8 solution containing fresh cell medium were placed into each 96-well microplate. After incubation of the CCK-8-treated samples for 2 h, their absorbance at 450 nm was recorded using a microplate reader.

Confocal-Laser-Microscopy Analysis: HeLa cells (2×10^5) were seeded on clean coverslips in a 6-well plate, followed by incubation for 24 h at 37 °C. The cells were rinsed using PBS, and sQDs or Si@QDs@Si NPs were then treated into the cells, and incubated for 24 h. The sQD- or Si@QDs@Si NP-treated HeLa cells were fixed using 4% polyoxymethylene solution (Wako, Pure Chem., Osaka, Japan) under mild shaking conditions for 20 min. Cells were vigorously washed three times using PBS, and attached onto the coverslip using a mounting solution containing 2-(4-amidinophenyl)-1H-indole-6-carboxamidine (4′,6-diamidino-2-phenylindole) (DAPI) solution (Vector Laboratories, Inc, CA). Confocal microscopy images were analyzed using a Zeiss LSM image examiner (for DAPI imaging, excitation wavelength: Haupt-Farb-Teiler (HFT) 405/488 nm, pinhole diameter: 92 µm, filter: BP 420-480 IR; for QD imaging, HFT 405/488/543/633 nm, pinhole diameter: 110 m, filter: 604-754).

In Vivo Fluorescence Imaging in the Xenograft Tumor Model: Si@QDs@Si NPs or sQDs (2 pmole) in PBS solution were prepared after washing followed by centrifugation. HeLa cells (1×10^6) in a 10 cm flask dish were incubated for 24 h and mixed with the as-prepared Si@QDs@Si NPs or sQDs for 24 h. The harvested HeLa cells, in 100 µL of PBS, after trypsinization, were subcutaneously implanted into both thighs of a 6-week-old male nude (nu/nu) mouse. Each male mouse was anesthetized via an intraperitoneal injection of ketamine (50 mg kg^{-1}) and xylazine (2.5 mg kg^{-1}). In vivo fluorescence imaging experiments were conducted using a Maestro optical imaging system (CRi Inc., Woburn, MA, USA). For in vivo QD studies, the fluorescence imaging filters were

set as a green filter (a band-pass filter ranging from 503 to 555 nm, and a long-pass filter of 580 nm) with 0.2 s exposure. Autofluorescence signals from skin or food were removed by the Maestro software using a spectral unmixing program.

Optical Characterization: UV–vis absorption spectra were recorded using a UV-vis spectrometer. Fluorescence quantum yields and photoluminescence (PL) spectra (Figure 1) were recorded using a 6500 photoluminescence spectrometer (JASCO).

Optical UV Stability: QD samples were exposed to a UV-irradiation source to monitor their UV stability. The distance between the samples and the UV lamp was 10 cm. The variation in wavelength shift was less than 5% after exposure to UV for 3000 h.

Supporting Information

Supporting Information is available from the Wiley Online Library or from the author.

Acknowledgements

B.-H.J. and D.W.H. contributed equally to this work. This work was supported by the Bio & Medical Technology Development Program of the National Research Foundation (NRF) funded by the Korean government (MEST) (No. 2011-0029945), and WCU project of the MEST and the NRF (R31-2008-000-10103-0), and the National Research Foundation of Korea (NRF) grant (2011-0019044).

Received: December 3, 2011
Published online: February 17, 2012

[1] M. K. Wagner, F. Li, J. J. Li, X. F. Li, X. C. Le, *Anal. Bioanal. Chem.* **2010**, *397*, 3213.
[2] C. Carrillo-Carrion, S. Cardenas, B. M. Simonet, M. Valcarcel, *Chem. Commun.* **2009**, 5214.
[3] K. W. Johnston, A. G. Pattantyus-Abraham, J. P. Clifford, S. H. Myrskog, D. D. MacNail, L. Levina, E. H. Sargent, *Appl. Phys. Lett.* **2008**, *92*, 151115.
[4] M. Schierhorn, S. W. Boettcher, J. H. Peet, E. Matioli, G. C. Bazan, G. D. Stucky, M. Moskovits, *ACS Nano* **2010**, *4*, 6132.
[5] I. L. Medintz, A. R. Clapp, H. Mattoussi, E. R. Goldman, B. Fisher, J. M. Mauro, *Nat. Mater.* **2003**, *2*, 630.
[6] S. Coe, W.K. Woo, M. Bawendi, V. Bulovic, *Nature* **2002**, *420*, 800.
[7] B. H. Jun, G. Kim, M. S. Noh, H. Kang, Y. K. Kim, M. H. Cho, D. H. Jeong, Y. S. Lee, *Nanomedicine* **2011**, *6*, 1463.
[8] U. Resch-Genger, M. Grabolle, S. Cavaliere-Jaricot, R. Nitschke, T. Nann, *Nat. Methods* **2008**, *5*, 763.
[9] D. Gerion, F. Pinaud, S. C. Williams, W. J. Parak, D. Zanchet, S. Weiss, A. P. Alivisatos, *J. Phys. Chem. B* **2001**, *105*, 8861.
[10] E. I. Altinoglu, J. H. Adair, *WIREs Nanomed. Nanobiotechnol.* **2010**, *2*, 461.
[11] N. Ma, A. F. Marshall, S. S. Gambhir, J. H. Rao, *Small* **2010**, *6*, 1520.
[12] J. Kim, J.E. Lee, J. Lee, J. H. Yu, C. B. Kim, K. An, Y. Hwang, C. H. Shin, J. G. Park, J. Kim, T. Hyeon, *J. Am. Chem. Soc.* **2006**, *128*, 688.
[13] C. L. Wu, J. Zheng, C. Huang, J. Lai, S. Li, C. Chen, Y. Zhao, *Angew. Chem. Int. Ed.* **2007**, *46*, 5393.
[14] D. K. Yi, S. T. Selvan, S. S. Lee, G. C. Papaefthymiou, D. Kundaliya, J. Y. Ying, *J. Am. Chem. Soc.* **2005**, *127*, 4990.
[15] P. P. Pillai, S. Reisewitz, H. Schroeder, C. M. Niemeyer, *Small* **2010**, *6*, 2130.
[16] J. M. Behrendt, M. Afzaal, L. M. Alexander, M. Bradley, A. V. Hine, D. Nagel, P. O'Brien, K. Presland, A. J. Sutherland, *J. Mater. Chem.* **2009**, *19*, 215.
[17] H. S. Choi, W. Liu, F. Liu, K. Nasr, P. Misra, M. G. Bawendi, J. V. Frangioni, *Nat. Nanotechnol.* **2010**, *5*, 42.
[18] M. Cho, K. Lim, K. Woo, *Chem. Commun.* **2010**, *46*, 5584.
[19] R. G. Xie, U. Kolb, J. X. Li, T. Basche, A. Mews, *J. Am. Chem. Soc.* **2005**, *127*, 7480.
[20] J. Ouyang, B. Zaman, F. J. Yan, D. Jhonston, G. Li, X. Wu, D. Leek, C. I. Ratcliffe, J. A. Ripmeester, K. Yu, *J. Phys. Chem. C* **2008**, *112*, 13805.
[21] R. E. Bailey, S. M. Nie, *J. Am. Chem. Soc.* **2003**, *125*, 7100.
[22] C. Graf, S. Dembski, A. Hofmann, E. Ruhl, *Langmuir* **2006**, *22*, 5604.
[23] B. K. Pong, B. L. Trout, J. Y. Lee, *Langmuir* **2008**, *24*, 5270.
[24] J. B. Delehanty, C. E. Bradburne, K. Boeneman, K. Susumu, D. Farrell, B. C. Mei, J. B. Blano-Canosa, G. Dawson, P. E. Dawson, H. Mattoussi, I. L. Medintz, *Integr. Biol.* **2010**, *2*, 265.
[25] A. V. Naumova, H. Rainecke, V. Yarnykh, J. Deem, C. Yuan, C. E. Murry, *Mol. Imaging* **2010**, *9*, 201.
[26] H. R. Herschman, *Crit. Rev. Oncol. Hematol.* **2004**, *51*, 191.
[27] H. Kobayashi, M. Ogawa, N. Kosaka, P. L. Choyke, Y. Urano, *Nanomedicine* **2009**, *4*, 411.
[28] D. Sen, T. J. Deerinck, M. H. Ellisman, I. Parker, M. D. Cahalan, *PLoS One* **2008**, *3*, e3290.
[29] W. B. Cai, X. Y. Chen, *Nat. Protocols* **2008**, *3*, 89.
[30] G. Jiang, K. Park, J. Kim, K. S. Kim, S. K. Hahn, *Mol. Pharmaceutics* **2009**, *6*, 727.